Patch antenna microcavity terahertz sources with enhanced emission

J. Madéo,[1,2,a)] Y. Todorov,[2] A. Gilman,[1] G. Frucci,[2] L. H. Li,[3] A. G. Davies,[3] E. H. Linfield,[3] C. Sirtori,[2] and K. M. Dani[1]
[1]*Femtosecond Spectroscopy Unit, Okinawa Institute of Science and Technology Graduate University, 1919-1 Tancha, Onna, Japan*
[2]*Laboratoire Matériaux et Phénomènes Quantiques, Université Paris Diderot, Sorbonne Paris Cité, CNRS-UMR 7162, 75013 Paris, France*
[3]*School of Electronic and Electrical Engineering, University of Leeds, Woodhouse Lane, Leeds LS2 9JT, United Kingdom*

(Received 30 March 2016; accepted 20 September 2016; published online 4 October 2016)

We study the emission properties of an electroluminescent THz frequency quantum cascade structure embedded in an array of patch antenna double-metal microcavities. We show that high photon extraction efficiencies can be obtained by adjusting the active region thickness and array periodicity as well as high Purcell factors (up to 65), leading to an enhanced overall emitted power. Up to a 44-fold increase in power is experimentally observed in comparison with a reference device processed in conventional mesa geometry. Estimation of the Purcell factors using electromagnetic simulations and the theoretical extraction efficiency are in agreement with the observed power enhancement and show that, in these microcavities, the overall enhancement solely depends on the square of the total quality factor. *Published by AIP Publishing.*
[http://dx.doi.org/10.1063/1.4963891]

The ability to realize efficient sources and detectors at terahertz (THz) frequencies is of importance as this opens the way to a wide range of potential applications in molecular spectroscopy, imaging, security scanning, and in the fundamental studies of low energy chemical and physical processes.[1] For optoelectronic devices operating in the THz range, the light-matter interaction can be significantly enhanced by confining the electromagnetic field into highly sub-wavelength metallic structures. Effective volumes as low as $10^{-7}\lambda^3$, where λ is the radiation wavelength, have been achieved in passive double-metal micro-cavities comprising a dielectric layer bounded by a metallic back-plane and a patterned top metal layer.[2] Similarly, Purcell enhancement of spontaneous emission has been observed in LC microresonators as well as mirror-grating metal cavities[3,4] and microcavity effects for THz quantum cascade lasers have been discussed.[5,6] Double-metal confinement lends itself to the creation of arrays of patch antenna microcavities and has led to the demonstration of the ultra-strong light-matter coupling regime and the realization of efficient infrared and THz detectors.[7–9] In the case of square resonators, the resonant wavelength, λ, is set by the length of the square side, s, through the formula $s = \lambda/2n_{\text{eff}}$, where n_{eff} is the effective mode index. This photonic structure is ideal for intersubband (ISB) emitters as the oscillating dipoles of the electronic transition align with the intracavity *TM* mode polarization. In addition, this geometry behaves as a patch antenna, rotating the polarization of the confined field by 90° when radiating into the far-field. Therefore, one can realize surface emitting photonic devices in which the light-matter interaction can be enhanced by resonantly tuning the energy of the microcavity mode with a radiative ISB transition by adjusting only the geometric parameter s.[10]

In this letter, we study THz frequency emission from arrays of double-metal patch microcavities containing a quantum cascade (QC) active region. We demonstrate the enhancement of the electroluminescence owing to an efficient out-coupling that is achieved by carefully choosing the thickness of the active region in combination with large array periodicities. We investigated thin active regions ($L = 2\,\mu$m and $4\,\mu$m) as a function of the array period $p = d + s$ (where d is the distance between the two resonators), and the lateral resonator dimension, s. The active region is a GaAs/$Al_{0.15}Ga_{0.75}As$ QC electroluminescent design with a radiative ISB transition at 4.5 THz, similar to the structure described by Jasnot *et al.*[11] The layer sequence from the injection barrier is designed to be (in Angström, $Al_{0.15}Ga_{0.75}As$ barriers in bold) **44**/266/**40**/164/**22**/154/**22**/148/**24**/146/**26**/144/**28**/140/**34**/134, with the underlined GaAs wells Si doped at a concentration of 2×10^{16} cm^{-3}. Three different active region thicknesses were used for this work. The reference sample comprised 80 periods ($\sim 12\,\mu$m) and was processed in a single plasmon waveguide mesa with a 45° polished facet to out-couple the radiation. Two other structures comprising 27 periods ($\sim 4\,\mu$m) and 13 periods ($\sim 2\,\mu$m) were patterned into arrays of patch microcavities. All emission data were obtained by mounting the devices on the cold finger of a continuous flow helium cryostat, operating at a temperature of 10 K. Radiation was collected using 90° off-axis F#1 parabolic mirrors, allowing large collection angle and coupled to a helium-cooled bolometer. All devices were biased with a 10 kHz, 50% duty cycle modulation, gated by an 85 Hz square modulation to achieve lock-in detection with the bolometer.

Figure 1(a) shows an SEM picture of a typical device comprising a 13×13 array of ICP-etched patch resonators with lateral dimension $s = 11\,\mu$m, period $p = 26\,\mu$m, and an

a)Author to whom correspondence should be addressed. Electronic mail: julien.madeo@oist.jp

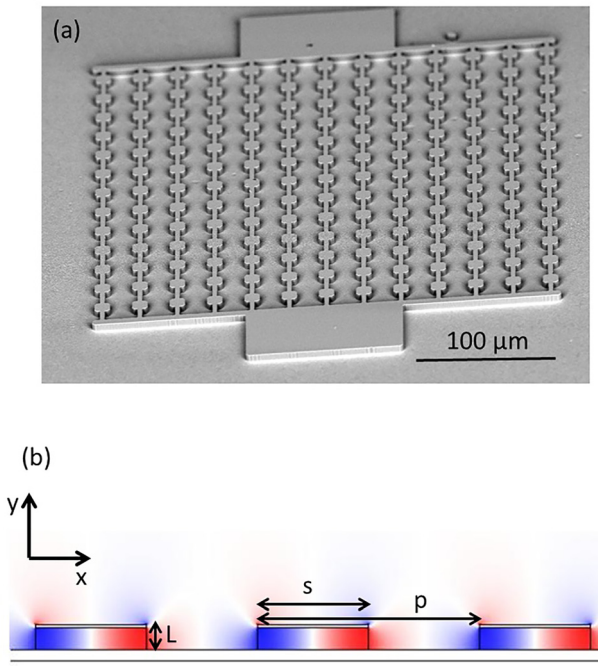

FIG. 1. (a) SEM picture of a fabricated device. (b) Electromagnetic simulation showing the field distribution of the *TM* confined modes for $s = 11\ \mu$m.

active region thickness $L = 4\ \mu$m. The upper surfaces of the resonators are connected by 2-μm-wide metal strips to ensure electrical injection into all elements of the array. Lateral contacts of size $50 \times 100\ \mu m^2$ were included for wire bonding, but kept as small as possible to limit their contribution to the emitted power.

We first demonstrated the increase of spontaneous emission by varying the lateral dimension s of the square patches, keeping the distance, d, between the resonators and number of resonators fixed. This tunes the micro cavity mode in and out of resonance with the ISB transition at 4.5 THz. The inset to Figure 2(a) shows the electroluminescence spectra for three devices with $s = 10\ \mu$m, $11\ \mu$m, and $12\ \mu$m, where $L = 4\ \mu$m and $d = 15\ \mu$m. The $s = 11\ \mu$m device shows the spectrally sharpest and strongest emission, whereas the two other devices exhibit a broader and complex spectral profile attributed to the detuning of the energy of the cavity mode from the electronic transition energy. This behaviour is consistent with the system operating in the weak coupling regime, with the observed enhancement of the spontaneous emission occurring through the Purcell effect.[3,4] This is further systematically revealed in Figure 2(a), which shows the I–V characteristics and measured optical power for the same active region as s is varied from 8 μm to 12 μm. The decrease in optical power for bias voltage above 1.3 V is attributed to a decoupling of the injection state with the upper state of the radiative transition, confirmed by band structure simulations (not shown).These data are summarized in Figure 2(b) and complemented with the results for two further values of the resonator spacing, $d = 5\ \mu$m and $d = 10\ \mu$m. This plot shows the maximum optical power as a function of the patch microcavity lateral size, s, for a current density of $\sim 50\ A/cm^2$ in all devices; both the $d = 10\ \mu$m and $15\ \mu$m curves show a clear resonance at $s = 11\ \mu$m. The $d = 5\ \mu$m curve is featureless, which is attributed to evanescent near-field coupling

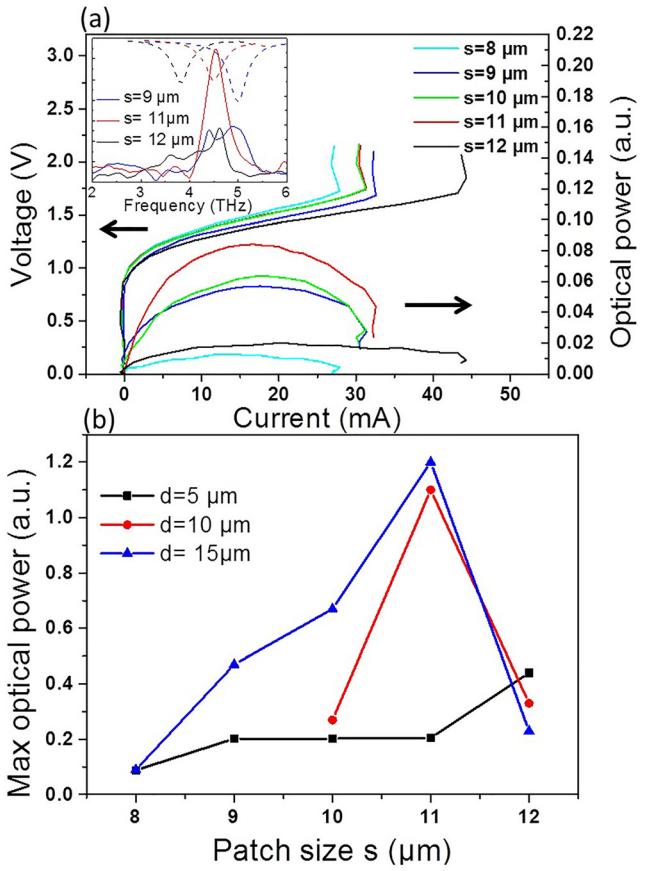

FIG. 2. (a) L-I-V characteristics as a function of lateral resonator size, s, for devices with $d = 15\ \mu$m and an active region thickness, $L = 4\ \mu$m. Inset: Measured emission and simulated reflectivity spectra for devices with $s = 9\ \mu$m, $11\ \mu$m, and $12\ \mu$m. (b) Optical power at a current density of $50\ A/cm^2$ for devices with $d = 5$, 10, and $15\ \mu$m as a function of lateral resonator size, s, showing the resonance for $s = 11\ \mu$m.

between the resonators.[2] All the following results of our study are performed with samples at resonance ($s = 11\ \mu$m) in order to be in the Purcell regime.

In Figure 3, the emission characteristics of the array devices are compared with that of the reference sample with an $L = 12\ \mu$m active region, fabricated in an $800 \times 800\ \mu m^2$ mesa with a 45° polished facet for photon emission. This geometry provides a very short effective photon propagation length ($l = L/\sin(45°) = 16.8\ \mu$m) allowing for the whole mesa surface to contribute to the emission. This is further confirmed by simulating the mode losses using Comsol ($\alpha = 12.1\ cm^{-1}$) providing negligible absorption ($\alpha l = 0.02$).The array spacing is $d = 15\ \mu$m for the $L = 4\ \mu$m sample and both $d = 25\ \mu$m and $d = 40\ \mu$m for the $L = 2\ \mu$m samples. In order to compare their relative performance, all data are normalized by the total volume of the device (total electrical area (A) $\times$ active region thickness (L)) to take into account the different sizes and active region thicknesses. A strong enhancement of the electroluminescence by more than one order of magnitude is observed between the mesa device and the microcavity emitters. The best performance is obtained for the device with the thinnest active region (2 μm) and the largest array spacing (d) of 40 μm.

To obtain a systematic study of the enhancement, we have measured the L-J characteristics (electroluminescent power versus current density) of all the samples discussed

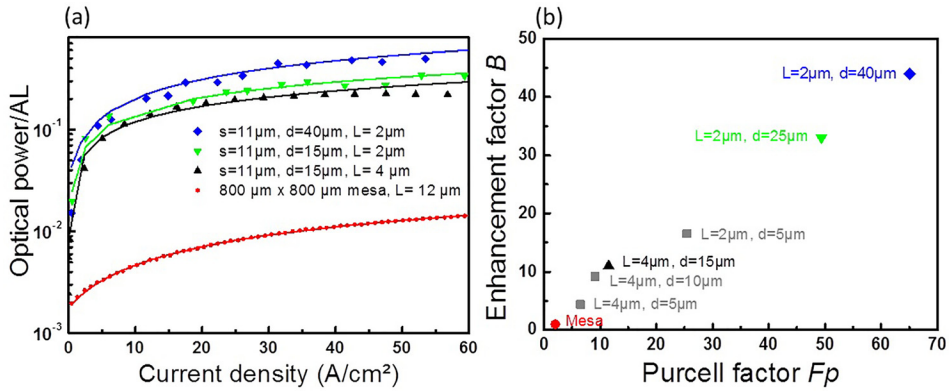

FIG. 3. Optical power normalized by overall device volume (total electrical area $A \times$ active region thickness L) as a function of injected current density for three patch microcavity array devices, and (red dots) a reference device fabricated in a mesa geometry. Fits are shown in solid lines. (b) Enhancement factor, B, as a function of Purcell factor for various devices.

above, with the electroluminescent signal normalized to the active region volume of the sample. Electroluminescence power from THz QC devices follows a square root dependence on the applied current density (instead of the usually linear behavior) as the dominant scattering mechanism arises from electron-electron interactions.[12] We have therefore fitted the L-J curves, corresponding to the total power integrated by the lock-in amplifier, with the function $y_0 + B\sqrt{J}$, where the coefficient B is related to the quantum efficiency of the sample, and with our choice of normalization, B is also the emission enhancement factor. y_0 accounts for offsets due to small electronic background. Only the first portion of the curves are fitted (bias range from 0.5 to 1.3 V) to avoid the effect of the structure misalignment reducing the optical power, as discussed above. A similar fitting protocol in the case of THz electroluminescence has been used in Ref. 4. Figure 3(b) summarizes the values of B compared to the reference mesa on a linear scale for various arrays fabricated for this study, as a function of the Purcell factor F_p, which is explained below (Eq. (1)). We observe that the enhancement is strongest for the thinnest samples ($L = 2\,\mu$m) with the largest array spacing, $d = 40\,\mu$m.

To understand the influence of the different geometrical parameters of the array on the emission, we need to understand the influence of photonic confinement (Purcell factor F_p) and photon recycling (quality factor Q). To this end, we performed electromagnetic simulations of the reflectivity curves for the arrays using a finite element method (COMSOL), which provide the modal characteristics of the structure.[10] The simulations were realized for an infinite array by using a simulation box with periodic boundary conditions. For gold and GaAs, the complex refractive indices from Ref. 13 were used. The quality factors were extracted from the simulated reflectivity spectra by fitting with a Lorentzian profile. Figure 4(a) shows the quality factors, Q, for arrays with $L = 2\,\mu$m and $4\,\mu$m as a function of the distance, d, between the microcavities. There is a clear increase in Q as the period of the array is increased. The validity of the simulated quality factors is tested experimentally through reflectivity measurements on large arrays of patch microcavities of $3 \times 3\,\text{mm}^2$ with $L = 2\,\mu$m (shown in the inset of Figure 4(b)) using an FTIR spectrometer and a broadband source (Globar). Large arrays are used to enable a good signal-to-noise ratio, a large beam diameter, and to remove any parasitic contribution from the bonding contacts. The experimental data are in excellent agreement with the simulations. By varying the distance between resonators from 5 to 40 μm, the quality factor Q is improved by approximately a factor of three. The inset of Figure 4(a) shows the quality factors obtained from the simulation for different thickness L of the resonators at fixed s (11 μm) and d (40 μm). We observe that the quality factor is maximum for L around 2 μm, explaining our choice for studied devices' thicknesses. Lower Q for $L < 2\,\mu$m is attributed to increased ohmic losses and reduced radiative losses, i.e., stronger overlap of the cavity mode with the lossy metallic layers owing to the higher confinement. Lower Q for $L > 2\,\mu$m thickness is attributed to increased radiative losses and reduced ohmic losses.

This improvement affects directly the Purcell factor F_p, which is expressed in the present case as[3,14]

$$F_p = \frac{3}{4\pi^2}\left(\frac{\lambda}{n}\right)^3 \frac{Q}{V}, \tag{1}$$

where λ is the vacuum emission wavelength, n is the refractive index of the cavity mode, and V is the volume of a patch, $V = Ls^2$. Besides, the expression of the Purcell factor is the same for a single resonators and an array of resonators for which the optical modes are strongly localized.[15]

Figure 4(b) shows the estimated Purcell factors for $L = 2\,\mu$m and $L = 4\,\mu$m as a function of distance, d, between resonators. The highest Purcell factor $F_p = 65$ is obtained for the thinnest micro cavities with $L = 2\,\mu$m, and for the largest value of d (=40 μm). Indeed, this array combines the highest quality factor $Q = 25$ observed in dilute arrays with the smallest volume $V = 242\,\mu\text{m}^3$. The Purcell factor thus has a very similar dependence on the geometrical parameters of the arrays as that observed with the experimental values of B in Fig. 3(b). However, in order to estimate the overall emission enhancement contained in the coefficient B, the photon extraction efficiency must be considered alongside the Purcell factor. The extraction efficiency is defined as Q/Q_{rad}, where Q_{rad} is related to the radiation loss of the structure. It can be extracted from the experimental data via

$$\frac{Q}{Q_{rad}}(\text{exp.}) = \frac{F_{p,mesa}T_{mesa}}{F_{p,patch}}\frac{B_{patch}}{B_{mesa}}, \tag{2}$$

where $F_{p,mesa}$ and $F_{p,patch}$ are the Purcell factors of the mesa and the patch antenna devices, respectively. T_{mesa} is the transmission coefficient through the polished facet of the mesa, and B_{patch} and B_{mesa} are the enhancement factors. The value of $F_{p,mesa}T_{mesa}$ is close to 1. Indeed, the enhancement of the

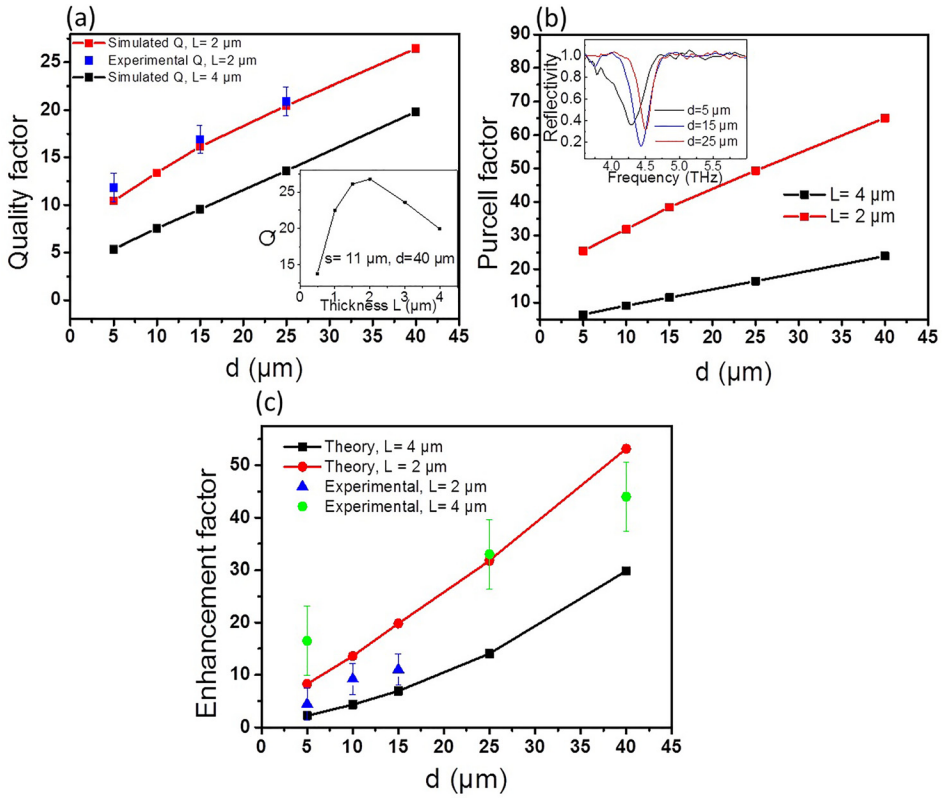

FIG. 4. (a) Quality factors deduced from the simulated reflectivity spectra for $L = 2\,\mu$m and $L = 4\,\mu$m, and experimental quality factors (blue squares) for $L = 2\,\mu$m and $d = 5$, 15, and 25 μm. Inset: Simulated quality factor as a function of the cavity thickness for $s = 11\,\mu$m and $d = 40\,\mu$m. (b) Estimated Purcell factors from the simulations for $L = 2\,\mu$m and $L = 4\,\mu$m. Inset: Experimental reflectivity spectra. (c) Comparison between experimental and theoretical enhancement factor (F_pQ/Q_{rad}) for $L = 2\,\mu$m and 4 μm.

power emitted by a single dipole embedded in the array with respect to a dipole in free space is provided by the product F_pQ/Q_{rad}. This quantity reflects the acceleration of the spontaneous emission weighted by the photon out-coupling efficiency and is defined as the emission enhancement factor B determined from our experiments, but instead of a free space dipole, we have an edge emitting mesa device. Because of the top metal layer, and the direction of the emitting dipole that is perpendicular to the metal, the Purcell factor for the mesa device is given by $F_p = 2$.[16] The photon out-coupling is given by the transmission coefficient of the polished facet $T = \frac{4n}{(1+n)^2}$, which is of the order 0.7, with $n = 3.6$. In reality, the photon out-coupling efficiency is lower as the transmission has to be integrated over the entire dipole radiation pattern. We can thus assume that the enhancement factor of the mesa to be $B_{mesa} \sim 1$.

We compare the experimental and theoretical extraction efficiency in Table I. To calculate the theoretical value of the extraction efficiency, Q was determined by electromagnetic simulations (Fig. 4(a)) and Q_{rad} by the relation[17]

$$Q_{rad} = \frac{\pi\lambda^3}{16 \times 3.8V} \tag{3}$$

TABLE I. Comparison between theoretical and experimental extraction efficiency Q/Q_{rad}.

L(μm), d(μm)	Q/Q_{rad} (theory)	Q/Q_{rad} (exp.)
4, 5	0.83	0.68
4, 10	0.82	0.97
4, 15	0.8	0.95
2, 5	0.66	0.65
2, 25	0.48	0.66
2, 40	0.41	0.67

Note that the dependence $Q_{rad} \sim \lambda^3/V$ is similar to that expected for the case of electrically small antennae.[18,19] The experimental and theoretical extraction efficiencies are in reasonable agreement and demonstrate very high photon out-coupling. By comparison, only a few percent extraction efficiencies have been previously reported in the case of rectangular shaped patch microcavities with strong lateral confinement along one direction leading to significantly higher radiative quality factors.[17] We note that the experimental Q/Q_{rad} is generally higher than the prediction, which can be attributed to an antenna effect from the 2-μm-wide wires connecting the resonators that enhance the photon out-coupling. On the other hand, the reference sample owing to a single plasmon confinement is expected to show lower losses than the double metal microcavities,[20] which would lead to an underestimation of the Purcell factor. Furthermore, the proximity of absorbing layers, i.e., the doped contact layers of the structure could increase the spontaneous emission rate, a phenomenon known from the fluorescence of molecules close to an absorbing metal mirror.[16]

In Figure 4(c), we compare the theoretical enhancement factor F_pQ/Q_{rad} with the values from Fig. 3(b). By taking the product of Eqs. (1) and (3), the total enhancement factor can be reduced to

$$F_p\frac{Q}{Q_{rad}} = \frac{12Q^2}{4\pi^3 n}, \tag{4}$$

which only depends on the squared total quality factor of the patch array. A good agreement is obtained, although the theoretical model underestimates the extraction efficiency, as discussed above. It reveals that in such structures the emission is mainly governed by the overall quality factor Q and not by the aspect ratio of the resonator. The

dependence of the emission on the geometrical parameters, such as thickness and array periodicity, appears mainly in the dependence of the quality factor on these parameters, as shown in Fig. 4(a).

In conclusion, we demonstrate enhanced electroluminescence in arrays of double-metal patch microcavities with an up to 44-fold improved performance when compared to a device with the active region in a mesa geometry, according to the results from Figs. 4(b) and 4(c). The origin of this improvement is attributed to high Purcell factors (of up to 65) increasing the spontaneous emission rate owing to the small volume of the microcavities, as well as higher quality factors as the array period is increased. In addition, we show in these structures significantly better photon extraction efficiency than reported in previous studies which can be controlled via the array period and the thickness of the resonator. This design provides a way to achieve efficient surface emitting THz sources. Possible further investigations would include the realization of surface emitting quantum cascade lasers in which control of the losses would be of interest to access higher optical powers. Such devices, with elongated resonators coupled to an external cavity, have been recently reported but only in the case of a thick active region ($>10\,\mu$m) and much larger modal volume.[21] Considering the high field confinement and hence high power densities enabled by square patch microcavities, these are a promising means to realize sources based on optical nonlinearities, such as up conversion or second harmonic generation.[22–24]

We acknowledge financial support from ANR-11-NANO-0020 project Delta, and the Engineering and Physical Sciences Research Council [EP/J017671/1, "COTS"]. We also acknowledge support from the Royal Society and Wolfson Foundation.

[1]M. Tonouchi, Nat. Photonics **1**, 97 (2007).
[2]C. Feuillet-Palma, Y. Todorov, R. Steed, A. Vasanelli, G. Biasol, L. Sorba, and C. Sirtori, Opt. Exp. **20**(27), 29121 (2012).
[3]C. Walther, G. Scalari, M. Beck, and J. Faist, Opt. Lett. **36**(14), 2623 (2011).
[4]Y. Todorov, I. Sagnes, I. Abram, and C. Minot, Phys. Rev. Lett. **99**, 223603 (2007).
[5]S. Kumar and Q. Hu, Appl. Phys. Lett. **100**, 041105 (2012).
[6]E. Strupiechonski, D. Grassani, D. Fowler, F. H. Julien, S. P. Khanna, L. Li, E. H. Linfield, A. G. Davies, A. B. Krysa, and R. Colombelli, Appl. Phys. Lett. **98**, 101101 (2011).
[7]Y. Todorov, A. M. Andrews, I. Sagnes, R. Colombelli, P. Klang, G. Strasser, and C. Sirtori, Phys. Rev. Lett. **102**, 186402 (2009).
[8]Y. N. Chen, Y. Todorov, B. Askenazi, A. Vasanelli, G. Biasol, R. Colombelli, and C. Sirtori, Appl. Phys. Lett. **104**, 031113 (2014).
[9]D. Palaferri, Y. Todorov, Y. N. Chen, J. Madeo, A. Vasanelli, L. H. Li, A. G. Davies, E. H. Linfield, and C. Sirtori, Appl. Phys. Lett. **106**, 161102 (2015).
[10]Y. Todorov, L. Tosetto, J. Teissier, A. M. Andrews, P. Klang, R. Colombelli, I. Sagnes, G. Strasser, and C. Sirtori, Opt. Exp. **18**(13), 13886–13907 (2010).
[11]F.-R. Jasnot, L.-A. de Vaulchier, Y. Guldner, G. Bastard, A. Vasanelli, C. Manquest, C. Sirtori, M. Beck, and J. Faist, Appl. Phys. Lett. **100**, 102103 (2012).
[12]M. Rochat, J. Faist, M. Beck, U. Oesterle, and M. Ilegems, Appl. Phys. Lett. **73**(25), 3724 (1998).
[13]E. D. Palik, *Handbook of Optical Constants of Solids* (Elsevier, 1997).
[14]A. V. Kavokin, J. J. Baumberg, G. Malpuech, and F. P. Laussy, *Microcavities* (Oxford University Press, 2007).
[15]H. Iwase, Y. Gong, D. Englund, and J. Vuckovic, *Nanoscale Photonics and Optoelectronics* (Springer, 2010), Chap. 1.
[16]R. R. Chance, A. H. Miller, A. Prock, and R. Silbey, J. Chem. Phys. **63**(4), 1589 (1975).
[17]C. Feuillet-Palma, Y. Todorov, A. Vasanelli, and C. Sirtori, Sci. Rep. **3**, 1361 (2013).
[18]L. J. Chu, J. Appl. Phys. **9**, 1163–1175 (1948).
[19]J. S. McLean, IEEE Trans. Antennas Propag. **44**, 672–675 (1996).
[20]B. S. Williams, S. Kumar, H. Callebaut, L. Reno, and Q. Hu, Appl. Phys. Lett. **83**, 2124–2126 (2003).
[21]L. Xu, C. A. Curwen, P. W. C. Hon, Q.-S. Chen, T. Itoh, and B. S. Williams, Appl. Phys. Lett. **107**, 221105 (2015).
[22]M. A. Belkin, F. Capasso, A. Belyanin, D. L. Sivco, A. Y. Cho, D. C. Oakley, C. J. Vineis, and G. W. Turner, Nat. Photonics **1**, 288–292 (2007).
[23]J. Madéo, P. Cavalié, J. R. Freeman, N. Jukam, J. Maysonnave, K. Maussang, H. E. Beere, D. A. Ritchie, C. Sirtori, J. Tignon, and S. S. Dhillon, Nat. Photonics **6**, 519–524 (2012).
[24]J. Gambari, A. I. Fernandez-Dominguez, S. A. Maier, B. S. Williams, S. Kumar, J. L. Reno, Q. Hu, and C. C. Phillips, Phys. Rev. B **82**, 121303 (2010).